Affordable Wide-field Optical Space Surveillance using sCMOS and GPUs

Peter Zimmer
J. T. McGraw and Associates, LLC

John T. McGraw
J. T. McGraw and Associates, LLC

Mark R. Ackermann
J. T. McGraw and Associates, LLC

ABSTRACT

Recent improvements in sCMOS technology allow for affordable, wide-field, and rapid cadence surveillance from LEO to out past GEO using largely off-the-shelf hardware. sCMOS sensors, until very recently, suffered from several shortcomings when compared to CCD sensors – lower sensitivity, smaller physical size and less predictable noise characteristics. Sensors that overcome the first two of these are now available commercially and the principals at J.T. McGraw and Associates (JTMA) have developed observing strategies that minimize the impact of the third, while leveraging the key features of sCMOS, fast readout and low average readout noise.

JTMA has integrated a new generation sCMOS sensor into an existing COTS telescope system in order to develop and test new detection techniques designed for uncued optical surveillance across a wide range of apparent object angular rates – from degree per second scale of LEO objects to a few arcseconds per second for objects out past GEO. One further complication arises from this: increased useful frame rate means increased data volume.

Fortunately, GPU technology continues to advance at a breakneck pace and we report on the results and performance of our new detection techniques implemented on new generation GPUs. Early results show significance within 20% of the expected theoretical limiting signal-to-noise using commodity GPUs in near real time across a wide range of object parameters, closing the gap in detectivity between moving objects and tracked objects.

1. Introduction

Optical surveillance of near Earth space with global networks of small telescopes stands on the threshold of fundamentally changing the way SSA observations are carried out. The combination of small, wide-field optical systems carefully matched to fast, large area sensors and supported by efficient detection algorithms means that true surveillance is now not only feasible, but practical and affordable. Small telescopes are already profusing around the globe, though the vast majority of these are more traditional photometric and astrometric monitoring systems. True surveillance requires searching for things that you aren't already expecting.

sCMOS sensors are still maturing, but are not new. sCMOS sensors with the combination of properties here described are new. The results presented here are not by any means final; very rigorous sensor and system testing are still ongoing, but the ramifications of these technological developments will have important impact on the optical SSA community and it is in that spirit that these results are presented.

2. Summary of Previously Reported Results

In order to offer some insight into the performance into the capabilities of small optical detection systems, we refer to our previously reported results [1-5] and briefly summarized here:

- LEO objects are bright by astronomical standards
  - A 10cm sphere at 1000km appears ~12th magnitude (with Albedo A=1) to 14th magnitude (A=0.12)

- A golf ball (4.2cm) at 1000km range with a 90% albedo is ~14th magnitude
- Even under bright skies, a 16th mag. star is bright enough to detect in 1s with a 300mm telescope

- Objects in LEO have a high apparent angular velocity:
  - ~0.2 deg/s at 2000km, 0.4 deg/s at 1000km, and up to ~1.5 deg/s at 300km, observed near zenith.
  - Light from LEO objects is therefore trailed over many pixels, each of which contributes read noise and sky background noise – so-called trailing losses.
  - The resulting loss in per-pixel signal-to-noise ratio scales as the number of pixels in the streak, which can be hundreds to thousands of pixels long.

- Signal-to-noise (S/N) in the whole LEO streak is more significant than the per-pixel S/N by approximately the square root of the streak length
  - If you can find the streak it in the first place.
  - The low per-pixel S/N is most often ignored as part of the background by traditional source detection techniques because the per-detection-kernel S/N does not cross a statistical significance threshold.

- Rapid cadence (~1s) imaging with zero deadtime of wide instantaneous fields of view (FOV >> 1 square degree) can catch LEO objects as they streak through the field
  - Exposure time tailored so that a 1 deg/s object will cover half of the FOV.
  - Zero deadtime for maximum efficiency and no lost objects between exposures.
  - Optimize for existing hardware, read noise and feasibility of real time detection.
  - Detector deadtime from shuttering and readout of typical full-frame detectors has the same effect as an overall lower quantum efficiency.

- Astrometric and Photometric Performance of Proof-of-Concept Detection Systems
  - Each 2˚ x 3˚ FOV typically contains 1000+ UCAC4 astrometric standard stars
  - Typical astrometric residual w.r.t. UCAC4: 0.25-0.35 arcseconds rms
  - Limiting magnitude (6 sigma) for stars: ~15 for bright conditions, ~16 in dark skies in one second

- Example of Streak Detection Performance at LEO
  - 11.6 magnitude object moving 2,720 arcseconds per second detected at 8.6 sigma
  - Implied circular orbit altitude: 600km
  - Implied size: 20cm – assuming diffuse sphere with 0.12 albedo

- Example of Streak Detection Performance at MEO
  - Highly variable object, magnitude fluctuated dramatically between 11.3 & 13.2 over 15 seconds of dwell time in FOV
  - Apparent angular rate: 460 arcseconds per second.
  - Implied altitude: 4,435 km with inclination of 105˚
  - Intensity changed by factor of 4 in 2 seconds, and even faster within exposure time

- Parallax Range Determination
  - 27km separation of telescopes allows range determination in LEO and lower MEO and GTO regimes
  - Apparent parallax for object at 1000km is 1.5 degrees
  - 1 pixel (2.23") rms error in position in this case is ~750m range error
  - Larger baseline parallax can be useful at GEO ranges, with a 450 km baseline yielding ±10km range per measurement

- Previously reported Uncued LEO Mode Execution Time
  - 0.9s per 2x2 binned image, of which preprocessing takes 0.4s and detection code 0.5s
  - Star mask and noise model computed once per minute or as needed, taking up to 8 seconds
  - Typical time from detection to TLE generation: 4 seconds.

3. New sCMOS Developments

Recent developments in the sCMOS detector market, which is largely driven by microscopy systems, offer great promise for wide-field optical imaging of the sky. We describe these developments and some of their impacts. We are certainly not the first researchers to examine the potential of sCMOS sensors applied to the challenges of optical surveillance of space. Numerous other authors have examined sCMOS for astronomy, and at this conference over the

last few years (e.g. [6] but there are many others) several authors examined these sensors as applied to SSA related observations. The scope of this work is to analyze and summarize these new developments in commercially available sCMOS technology and point out a few of its idiosyncrasies.

Sensor Area/Size: Effective optical surveillance of the sky requires physically large active sensor areas. One of the biggest shortcomings of previously available sCMOS sensors is that they were fairly small, significantly limiting the useful field of view achievable with affordable telescope optics. The reason why this is not simply a free parameter in optimization is that, while the optical system focal length can be tailored over a wide range, optical systems with focal ratios faster than f/2 become increasingly expensive. Sometimes this extra expense is worth the resulting costs, but as systems become even faster, it rapidly becomes impractical except perhaps as a development exercise. In this way, sensor size becomes the critical limit of system performance. The nature of these sensors also does not readily allow for close packing of sensor mosaics because much of the readout electronics are adjacent to the active area on the same substrate.

Front illuminated sCMOS sensors are available in very large formats, up to 165mm x 27mm, but these still have lower quantum efficiency and have somewhat higher read noise due to their size. Under some circumstances, even with these limitations these sensors may still have appropriate performance. Back-illuminated sensors are available in sizes up to 22 x 22 mm, roughly 60% of the area of a standard 35mm CCD, and it is this device that the remainder of this section will focus on. While still not as large as commonly available CCDs, this is more than made up for in sensitivity. However, applications that require very large area *and* high quantum efficiency will still require backside illuminated CCDs. Figure 1 shows the layout of the GPixel Gsense400BSI package, available in cameras from several manufacturers.

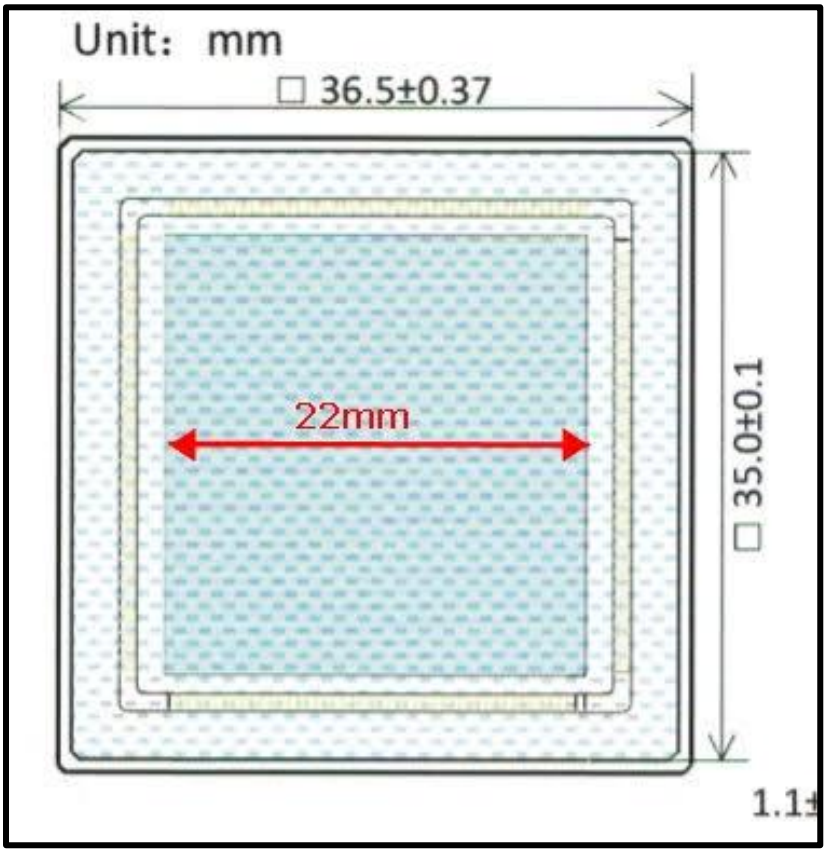

Figure 1 shows a diagram of relative sizes of the GPixel Gense400BSI-TVISB.

Quantum Efficiency: The second significant advancement is back-side illuminated architecture. Obviously this is not strictly a new development because astronomical CCDs have been thinned for backside operation for decades. The combination of sensor size and backside illumination in commodity camera systems *is* new. Figure 2 compares

quantum efficiency of these sCMOS detectors and the previous sensors used in JTMA's systems, which have a quantum efficiencies that are fairly typical of detectors widely in operation. This gain in sensitivity alone accounts for a substantial detectivity increase over our previous work.

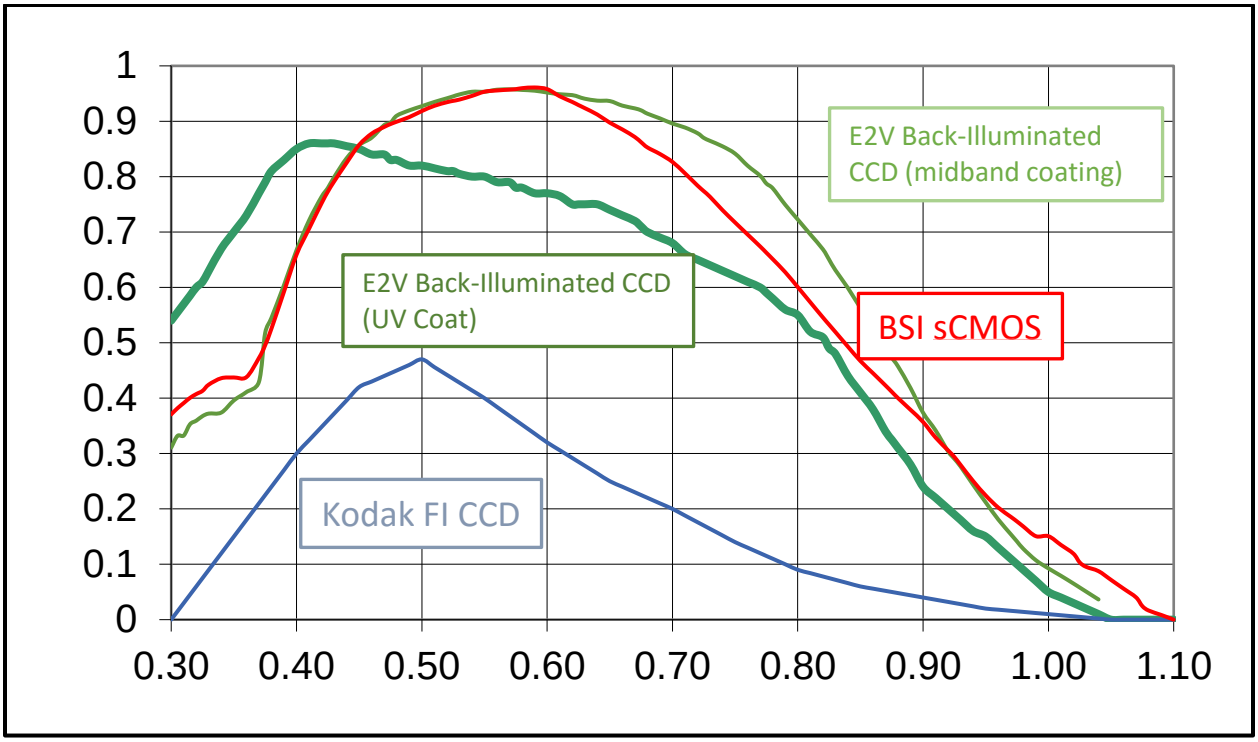

Figure 2 – These graphs show the typical sensor quantum efficiencies for various archetypical CCD sensors frequently encountered at astronomical observatories and those on which we've previously reported. The backside illuminated sCMOS is plotted on top of these and shows that is compares favorably with even some of the best CCD sensors available.

Read Noise: For streak detection, lower read noise is a critical factor. Compared to the sensors we've reported on previously, interline, front-illuminated CCDs, the read noise is at least a factor of 6 lower. More importantly is the noise variance, smaller by a factor of 40, because it is the ratio of sky noise variance to read noise that is critical. So lower read noise means one can be sky noise dominated in darker sky backgrounds. It is important to note that, because each pixel has its own set of amplifiers, the read noise is different for each pixel and shows a roughly log-normal distribution. That means there can be a few pixels with very large read noise. This can be problematic for streak detection, because a single very hot pixel can overwhelm the noise of all the others. Figure 3 shows the measured noise distribution and cumulative distribution for the deployed backside sCMOS sensor based on a large series of 20 μs exposures. This distribution is slightly but systematically higher, 2.1 e-, than the expected specification with a modal value of 1.5 e-, which is probably due to this being an early generation sensor and the general optimism of specification writers.

Other detector properties analogous to bias and flat response are also variable from pixel to pixel with a similar log-normal-looking curve and are correlated along rows. In much the same way that a few very hot pixels can dramatically affect streak finding efficiency, systematic structures in the background can look like streaks from real objects. When compared to contemporary CCD imagery, the sCMOS images are cosmetically much more complicated and more pre-processing operations are needed to counter these instrumental signatures. Figures 4 & 5 show an example results from such a cleaning process. Figure 4 shows the sum of 64 unprocessed sky frames. The summation was required to show the lower level fixed pattern structure that in individual frames is less apparent due to the background noise. Structures like these can contribute significant power to false positive detections in streak finding applications. Figure 5 shows the same region as in Figure 4, but in this case it is the summed stack of 64 processed sky frames. The processing corrects for each individual pixel's bias as well as masking stars and hot/noisy pixels. The resulting frames are free of systematic structures at levels that significantly impact streak detection.

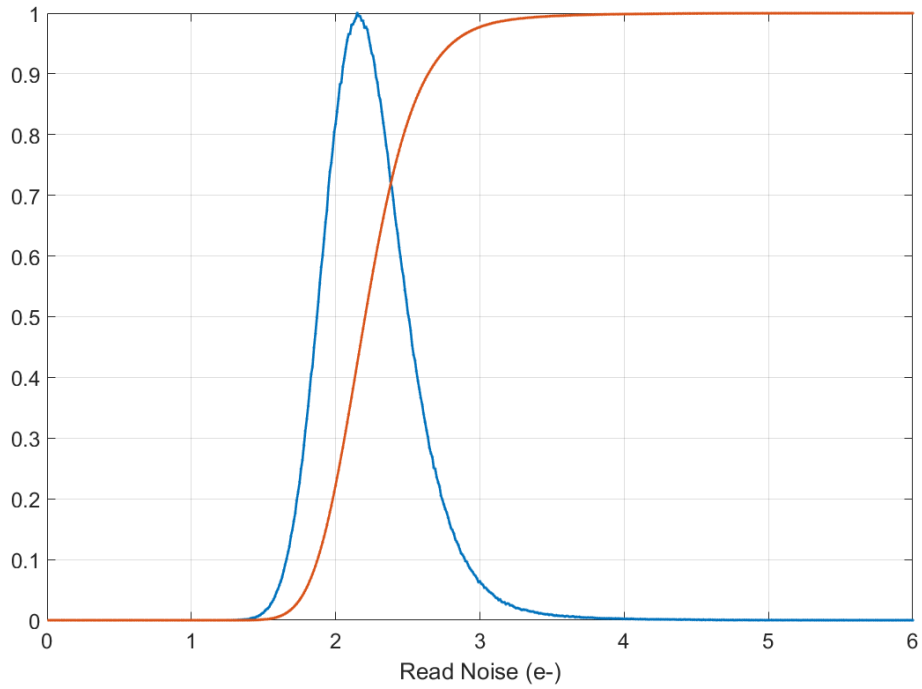

Figure 3 – These graphs shows the measured read noise distribution (blue) and cumulative distribution (red) for the deployed backside illuminated sCMOS sensor.

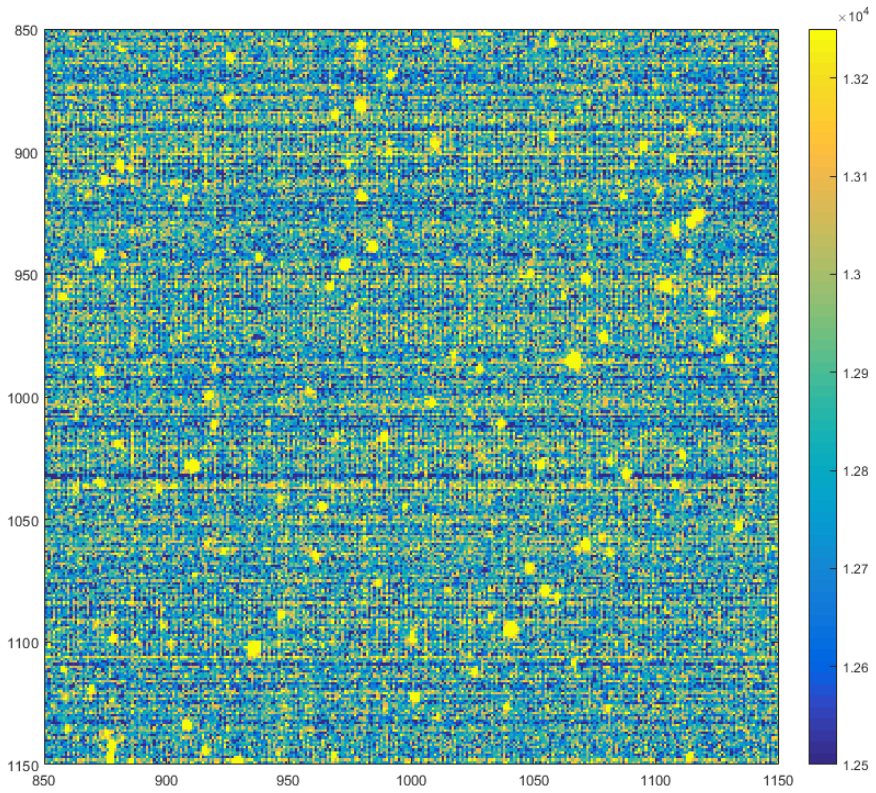

Figure 4 – This figure shows a small region taken from the middle of a summed stack of sCMOS images. The summation is required to make the fixed pattern structures apparent.

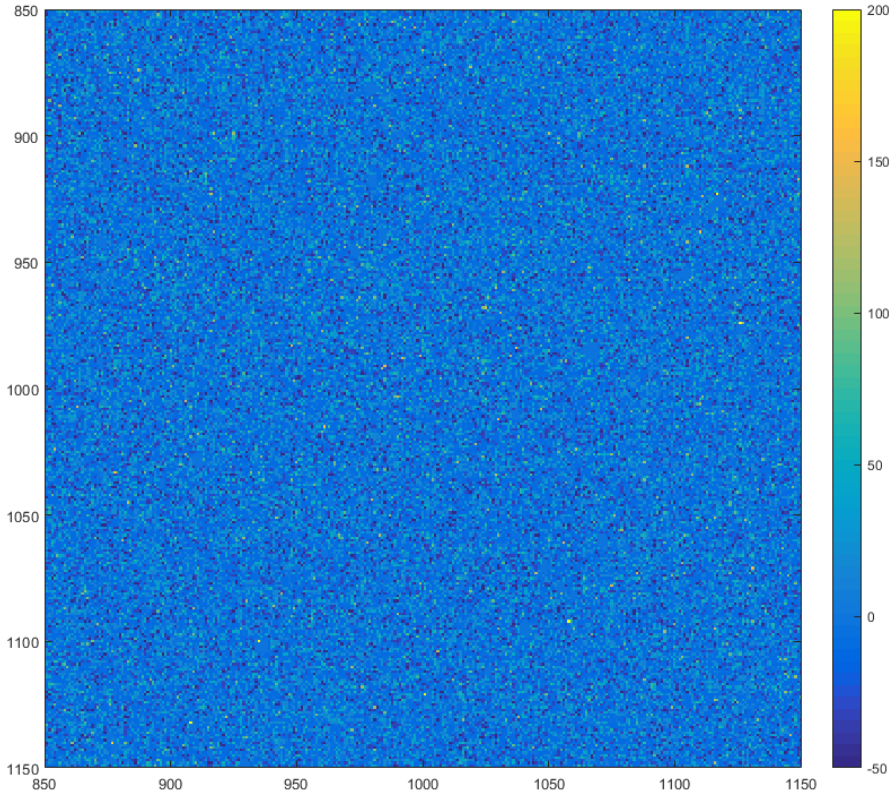

Figure 5 – This figure shows the same data set as Figure 4 but in this case each pixel has had the equivalent of a CCD bias removed. Stars and bad pixels, totaling roughly 2.5% of the total pixels, have been masked. For streak detection applications, this must be done with great care so as to minimally disturb the pixel noise distribution.

Data Rate: The frame rate of earlier CCDs could be quite high, but the read noise continued to increase, negating the advantage. Thus we always limited our systems to 1 frame per second (fps) even though they could run faster. The sCMOS sensors are limited by the row read time of 20us – 20us x 2048 rows yields ~25fps without imparting the read noise.

More measurements, presuming they are robust, is unequivocally a good thing. In this case, they enable all new streak finding methods. But once again these data rates put real time streak detection into new regimes of computational demands. Fortunately GPUs come to the rescue again. It does no good to design small, deployable, inexpensive optical survey systems if each one requires a supercomputing cluster on site. Continued performance increases that follow Moore's Law scaling mean that the GPUs we now use in our baseline systems are 60% faster each than those sold last year. 50 Tflops in a typical desktop chassis costs significantly less than the camera it is supporting.

4. Baseline System with sCMOS

The underlying telescope system is largely unchanged from our previous work. The optical system is a Celestron C-14 fitted with a Hyperstar prime-focus corrector, which operates at f/1.9 and delivers a 1.88˚ x 1.88˚ field of view onto the GPixel GSense400BSI sensor. The sensor is housed in a Tucsen Dhyana 95 camera which is operated via USB 3.0, which is required for the high data rate. The image data are read off and immediately corrected as per Figure 5 before being sent to the GPU processing system for streak detection and characterization.

5. Some Initial Measurements

We present our first light measurements of a piece of Iridium 33 debris (NORAD 33869) that passed through one of our early image sets on the night of Sept 16, 2016, which unfortunately corresponded to near Full Moon. While not normally the ideal circumstance for demonstrating telescope capability, hopefully it serves as a lower limit to overall performance.

The debris object was detected in 38 consecutive frames over 3.8s. As with most debris objects we observe, there is considerable variability in the source intensity, though at these sampling rates, some of this may be scintillation. Figure 6 shows an image cutout of a single 0.1s frame and Figure 7 shows the extracted light profile along the direction of travel.

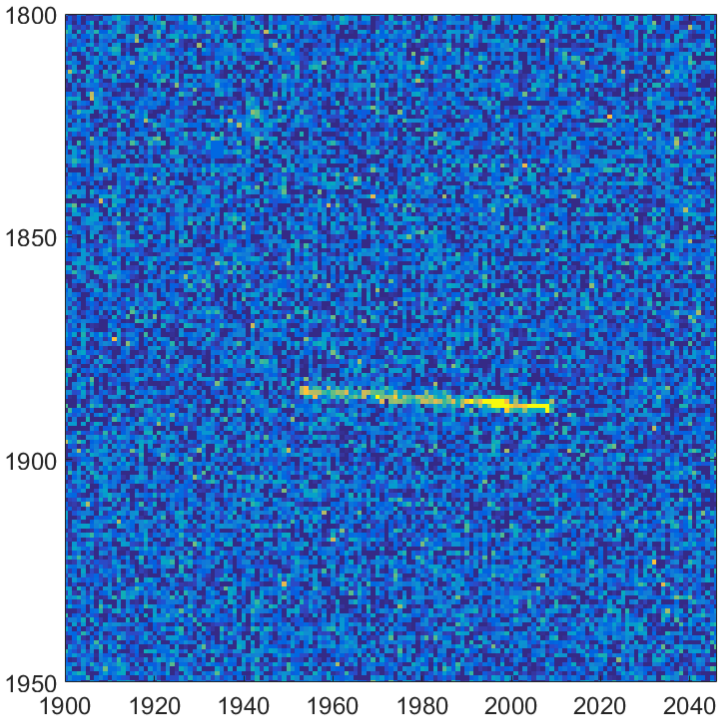

Figure 6 – This figure shows a small subsection of the processed (pixel bias, stars and hot pixels removed) 0.1s exposure time image containing one of 38 back-to-back detections of this Iridium 33 debris. This object was detected with a significance over 30σ in each frame.

The reason for choosing this particular detection is that the object is in an interesting orbital regime, with an altitude just under 825 km and it has a known radar cross-section. This debris object showed an apparent angular velocity of 1,856 arcseconds per second, consistent with that altitude. The brightness of the object shown in the above figure is magnitude ~11.4 based on photometric comparison to nearby stars in the field. The known radar cross-section of 0.08 m^2 which roughly translates to a diameter of 0.32m. At that range we expect a spherical diffuse reflector with albedo of 0.12 to be roughly magnitude 11.1. This is a somewhat larger discrepancy than we've seen in the past, but given the number of assumptions built in, it is not unreasonable.

These first results show that per 0.1s image the 6σ detectivity is approximately magnitude 13.3, or a roughly 15cm object at 1000km. JTMA's advanced detection algorithm pushes this well below 14th magnitude and we expect to be able to push it below 15th, or 6 cm at 1000 km.

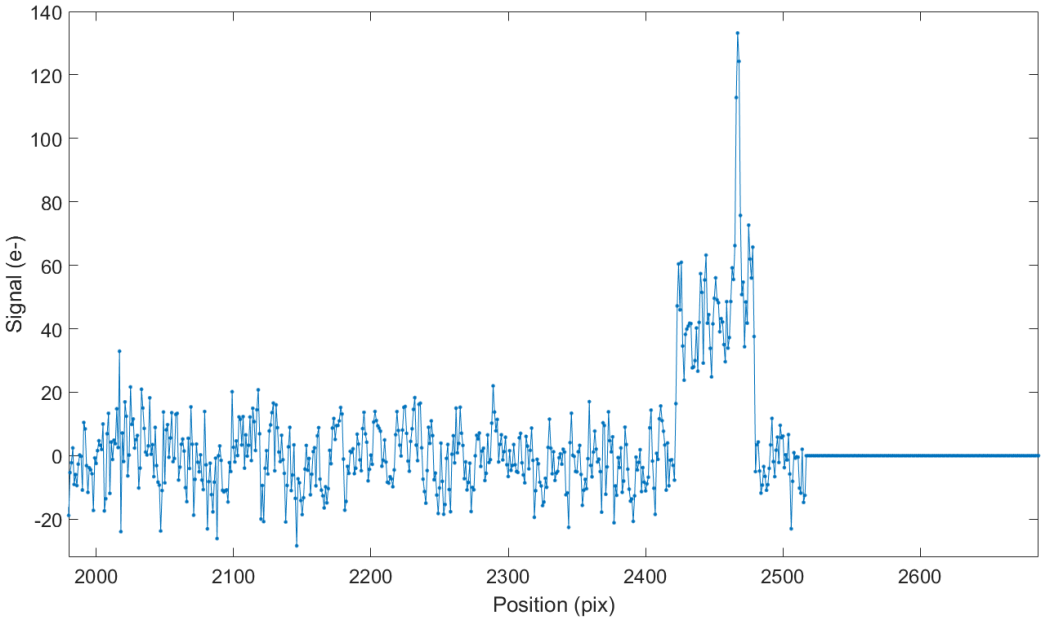

Figure 7 – This figure shows the extracted light profile of the Iridium debris detection.

Compared to our previous work, this one frame shows how much more sensitive this sensor is at detecting moving space objects. The high QE and lower read noise makes what had been a challenging detection only last year into one that's pretty easy for almost any streak detection technique. Figure 8 and 9 demonstrate this further. Figure 8 shows the co-addition of 10 frames to simulate a 1 second exposure. The image has been scaled to the noise so that the per-pixel detectivity is the same as in Figure 6. The extracted profile is shown in Figure 9, with the same profile as in Figure 7 over plotted. It is immediately apparent that trailing loss is making the per pixel signal to noise decrease as expected. The co-added streak is only marginally higher total signal to noise. This is shown in Figure 10 where the cumulative signal-to-noise ratio is calculated along each streak. The co-added streak is higher overall S/N, but not by the expected factor of the square root of 10 as if it were a point source.

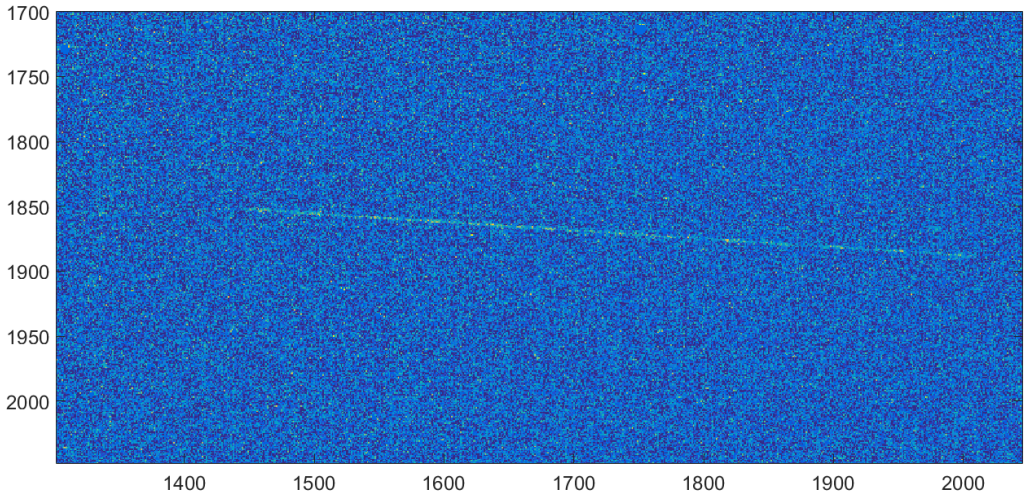

Figure 8 – This figure shows a co-addition of 10 0.1s exposures to simulate what this streak may have looked like to our old system. Even this is unfair though, because our old system would have had twice the noise variance per pixel because the read noise was so much higher.

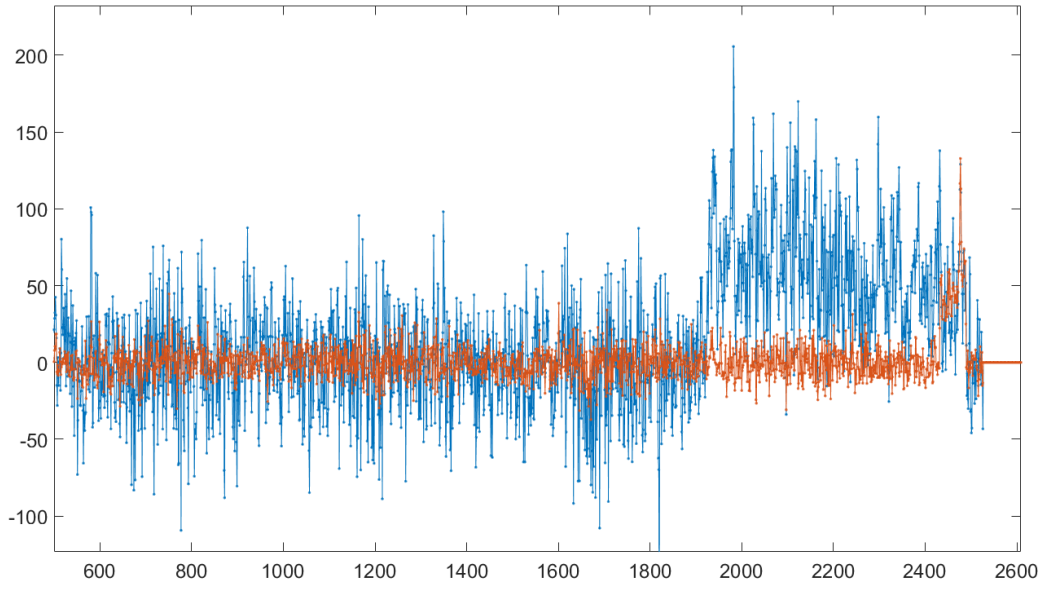

Figure 9 – This figure compares the light profile of the co-added ten frames shown in Figure 8 with the profile from Figure 7 superimposed. This is a great demonstration of trailing loss, showing how the sky noise is growing under the streak as exposures continue.

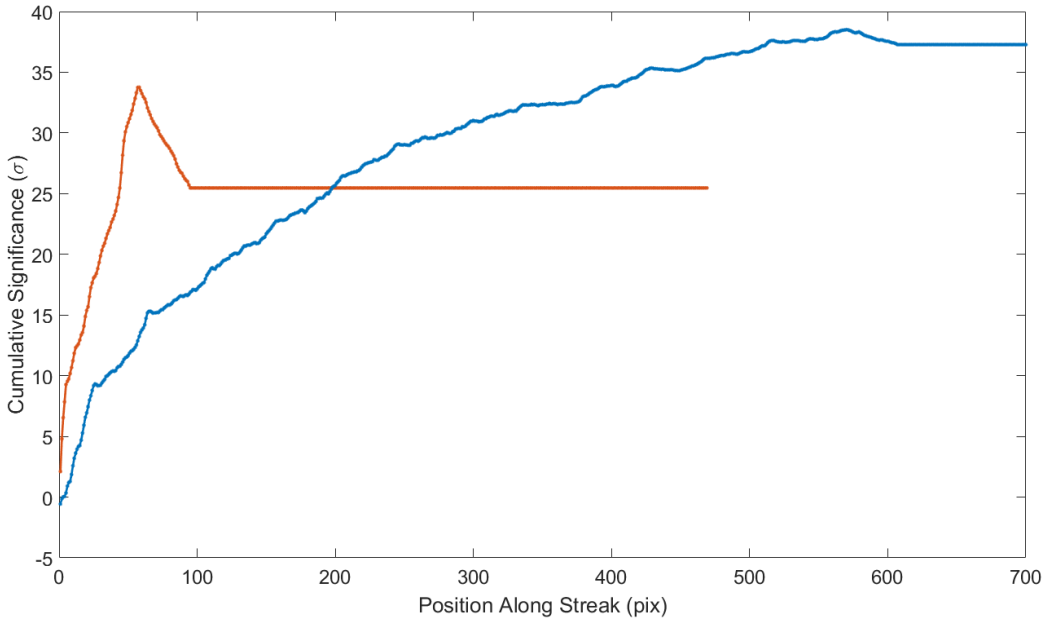

Figure 10 – This figure shows the growth in signal to noise along the streaks shown in Figures 6 & 8. They start from an identified end point and grow along the streak until the other end point, then fall off after that. The plateau at the end is the edge of the sensor. The salient point here is that the peak signal-to-noise in the co-added streak is only marginally higher than the single frame. It hasn't grown the way a point source would because of trailing loss. Rather it approaches an asymptote set by the target intensity and the ratio of read noise to sky noise.

6. Conclusions

We've shown an example uncued LEO detection but all of these techniques apply to objects in MEO, GEO, HEO and GTO. For slower objects, our magnitude limits of sensitivity increase dramatically, though the size of detectable object is necessarily larger because the signals fall off as R^2. Using these same data to predict performance at GEO the limits come out fainter than 17th magnitude, which is considerable for a 14" telescope. Especially given that these data were taken at Full Moon. Under dark skies, we expect this to improve dramatically and we continue to push our techniques to the limits that physics imposes.

JTMA continues to find new ways to push optical survey, telescope and detector technology to the problem of finding and measuring objects in near Earth space. Further work will continue to image the sky with these sensors as well as perform more rigorous tests of photometric performance. This new sCMOS technology is a game-changer and we can only wait expectantly for the next new innovation to come our way.

ACKNOWLEDGMENTS

The authors would like to thank Las Cumbres Observatory for lending us an earlier generation sCMOS camera for initial testing and development.

REFERENCES

[1] Zimmer, Peter C., McGraw, John T., Ackermann, Mark R., "GPU-based Uncued Surveillance from LEO to GEO with Small Optical Telescopes," *Proceedings of the 2015 AMOS Technical Conference*, 2015.

[2] Zimmer, Peter C., McGraw, John T., Ackermann, Mark R., "Demonstration of Uncued Surveillance of LEO*", Proceedings of the 2014 AMOS Technical Conference*, 2014.

[3] Zimmer, Peter C., Ackermann, Mark R., McGraw, John T. "GPU Accelerated Faint Streak Detection for Uncued Surveillance of LEO*", Proceedings of the 2013 AMOS Technical Conference*, 2013.

[4] Ackermann, Mark R., Kiziah, Rex R., Zimmer, Peter C., Beason, J. Douglas, Spillar, Earl J., Cox, David D., McGraw, John T., Vestrand, W. Thomas "Affordable Options for Ground-based, Large-aperture Optical Space Surveillance Systems," *Proceedings of the 2013 AMOS Technical Conference*, 2013.

[5] Zimmer, Peter C., McGraw, John T., Ackermann, Mark R., "GPU-based Uncued Surveillance from LEO to GEO with Small Optical Telescopes," *Proceedings of 2015 AAS/AIAA Astrodynamics Specialist Conference*, 2015.

[6] Schildknecht, Thomas "Improved Space Object Orbit Determination Using CMOS Detectors," *Proceedings of the 2015 AMOS Technical Conference*, 2015.